Front. Chem. Sci. Eng. 2020, 14(1): 61–75
https://doi.org/10.1007/s11705-019-1862-8

RESEARCH ARTICLE

4-Amino-1,8-naphthalimide based fluorescent photoinduced electron transfer (PET) pH sensors as liposomal cellular imaging agents: The effect of substituent patterns on PET directional quenching

Miguel Martínez-Calvo (✉)[1,3], Sandra A. Bright[1,2], Emma B. Veale[1], Adam F. Henwood[1], D. Clive Williams[2], Thorfinnur Gunnlaugsson (✉)[1]

1 School of Chemistry and Trinity Biomedical Sciences Institute (TBSI), Trinity College Dublin, The University of Dublin, Dublin 2, Ireland
2 School of Biochemistry and Immunology and Trinity Biomedical Sciences Institute (TBSI), Trinity College Dublin, The University of Dublin, Dublin 2, Ireland
3 Centro Singular de Investigación en Química Biolóxica e Materiais Moleculares (CIQUS) and Departamento de Química Orgánica Universidade de Santiago de Compostela, Rúa Jenaro de la Fuente s/n, 15782, Santiago de Compostela, Spain

Abstract Four new fluorescent sensors (**1**-**4**) based on the 4-amino-1,8-naphthalimide fluorophores (**Naps**) have been synthesized based on the classical fluorophore-spacer-receptor model. These four compounds all gave rise to emission bands centred at *ca.* 535 nm, which were found to be highly pH dependent, the emission being 'switched on' in acidic media, while being quenched due to PET from the amino moieties to the excited state of the **Nap** at more alkaline pH. The luminescent pH dependence for these probes was found to be highly dependent on the substitution on the imide site, as well as the polyamine chain attached to the position 4-amino moiety. In the case of sensor **2** the presence of the 4-amino-aniline dominated the pH dependent quenching. Nevertheless, at higher pH, PET quenching was also found to occur from the polyamine site. Hence, **2** is better described as a receptor$_1$-spacer$_1$-fluorophore-spacer$_2$-receptor$_2$ system, where the dominant PET process is due to (normally less favourable) 'directional' PET quenching from the 4-amino-aniline unit to the **Nap** site. Similar trends and pH fluorescence dependences were also seen for **3** and **4**. These compounds were also tested for their imaging potential and toxicity against HeLa cells (using DRAQ5 as nuclear stain which does now show pH dependent changes in acidic and neutral pH) and the results demonstrated that these compounds have reduced cellular viability at moderately high concentrations (with IC_{50} values between ca. 8–30 $\mu mol \cdot L^{-1}$), but were found to be suitable for intracellular pH determination at 1 $\mu mol \cdot L^{-1}$concentrations, where no real toxicity was observed. This allowed us to employ these as lysosomal probes at sub-toxic concentrations, where the **Nap** based emission was found to be pH depended, mirroring that seen in aqueous solution for **1-4**, with the main fluorescence changes occurring within acidic to neutral pH.

Keywords sensors, pH, photoinduced electron transfer, cellular imaging, confocal microscopy

1 Introduction

Intracellular pH plays a crucial role in many biological processes [1–5]. Consequently, the development of new tools for monitoring cellular pH with high selectivity and sensitivity is of great importance [6]. The 4-amino-1,8 naphthalimide (**Nap**) structure is a well-known building block often employed in the formation luminescent sensors based on the fluorophore-spacer-receptor based photo-induced electron transfer (PET) design [7]. These molecules are very sensitive to substitution at the 4-position of the **Nap** ring due to the "push-pull" nature of the internal charge transfer (ICT) excited state of the **Nap** (normally caused by the presence of an electron-donating amine and

Received February 28, 2019; accepted May 15, 2019

E-mails: gunnlaut@tcd.ie (Gunnlaugsson T),
miguel.martinez@usc.es (Martínez-Calvo M)

an electron-withdrawing imide), giving rise to a charge-separated excited state [8]. This property favours PET quenching of the excited state of the **Nap** by electron-rich receptors located at the 4-position [9]. The applicability of **Nap** compounds was broadly studied in our group in anion and cation sensing, and as DNA binders [10–13]. Recently, several researchers have employed **Nap** based structures for PET sensing of biologically relevant molecules or processes [14–16]. This includes the works of Sessler and co-workers, who developed probes for targeting the mitochondria [17], James and co-workers who developed probes for sugars [18], Qian and co-workers who formed many excellent examples of fluorescent **Nap** sensors for targeting both ions, and molecules, including DNA [19], and for observing cellular function [20], while Kelly and co-workers have made nucleic acid targeting pyridinium **Naps** [21,22]. James, Zhu, Gou and co-workers have developed many examples also of **Nap** based structures for sensing and monitoring biomolecules, drug delivery and intracellular function [23–25], while Pfeffer and co-workers have developed elegant examples of highly luminescent **Nap** sensors for sensing, imaging and medicinal applications [26,27]. Recently, the group of Magri has developed **Nap** based sensors capable of simultaneously monitoring pH and redox changes based on the fluorescent properties of ferrocene-**Naps** derivatives [28–30]. These examples demonstrate the wide range of applications of the **Nap** building block for biochemical applications. Such **Nap** systems are normally easily taken up into cells, and their cytotoxic nature can be modulated through simple structural design [24]. With this in mind we recently developed cellular imaging agents based on the **Nap** system, or so called pro-probes, where the **Nap** emission was used to monitor enzymatic processes in real time; this also resulting in the selective delivery of a therapeutic or imaging cargo into cancer cells [25]. The work presented herein is an extension to our aforementioned work, where the aim was the development of **Nap** based photoinduced electron transfer (PET) sensors that could monitor changes in the chemical environment of living cells [9,10,31–33], the structures of the four sensors **1**-**4** being shown in Fig. 1. Our aim is based on simply conjugating triethylenetetramine chains at the four position of the **Nap** ring, which results in the formation of pH sensors where protonation of the amines would reduce any intramolecular PET from the amine to the excited state of the **Nap** moieties, resulting in enhancement in their emission, and employing these in sensing or imaging of pH changes within cells. In particular, we were interested in developing structures that could sense changes within cancer cells, upon localising within their cytosol, which resulted in lysosomal localisation [24]. Herein, we present the outcome of our investigation, which included the analysis of the photophysical properties of **1-4** in both aqueous solution and biological media.

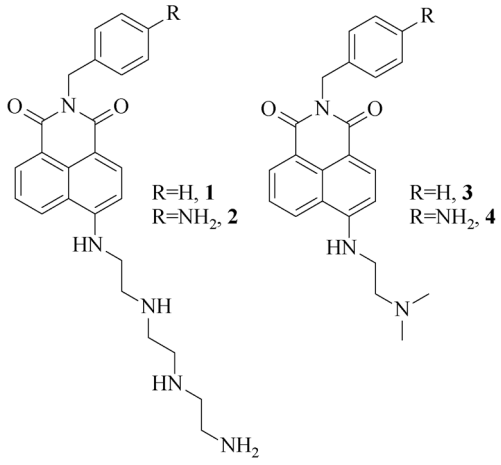

Fig. 1 The photoiniduced electron transfer (PET) **Nap** sensors **1-4** developed in this study.

2 Materials and methods

All solvents and chemicals were purchased from commercial sources and used without further purification. 4-Bromo-1,8-naphthalic anhydride, benzylamine, 4-aminobenzylamine and triethylenetetramine were purchased from Aldrich. Deuterated solvents used for NMR analysis (CD_3Cl, and $(CD_3)_2SO$) were purchased from Apollo Scientific. The ^1H NMR spectra were recorded at 400 MHz using a Bruker Spectrospin DPX-400 instrument. The ^{13}C NMR spectra were recorded at 101 MHz using a Bruker Spectrospin DPX-400 instrument. NMR spectra were also recorded using a Bruker AV-600 instrument operating at 600.1 MHz for ^1H NMR and 150.9 MHz for ^{13}C NMR. Chemical shifts are reported in ppm with the deuterated solvent as the internal reference. All NMR spectra were carried out at 293 K. Mass-spectrometry was carried out using HPLC grade solvents. Electrospray mass spectra were determined on a Micromass LCT spectrometer and high resolution mass spectra were determined relative to a standard of leucine enkephaline. Melting points were determined using an Electrothermal IA9000 digital melting point apparatus. Infrared spectra were recorded on a Perkin Elmer Spectrum One FT-IE spectrometer equipped with universal ATR sampling accessory. Elemental analysis was carried out on Exter Analytical CE440 elemental analyser at the microanalysis laboratory, School of Chemistry and Chemical Biology, University College Dublin.

2.1 Photophysical measurements

Otherwise stated, all measurements were performed at 298 K in 0.1 $mol \cdot L^{-1}$ NaCl solutions in water. The stock solutions of **1** and **2** were prepared in methanol (spectroscopic grade, Aldrich). UV-visible absorption spectra were measured in 1-cm quartz cuvettes (Hellma) on a Varian

Cary 50 spectrophotometer. Baseline corrections were applied for all spectra. Emission spectra were recorded on a Varian Cary Eclipse Fluorimeter. The temperature was kept constant throughout the measurements at 298 K by using a thermostated unit block. The data obtained were analysed using Origin 8.1®.

2.1.1 Spectrophotometric titrations and binding constants

The formation of the luminescent species was ascertained by fluorescent titrations of the corresponding solutions of **1** and **2** (5×10^{-6} mol·L^{-1}) with TBAOH (1, 0.1 and 0.001 mol·L^{-1}) and $HClO_4$ (1, 0.1 and 0.001 mol·L^{-1}) to vary the pH values between 2 and 10.

2.2 Cell culture

HeLa (human cervical cancer) cells were grown in Dulbecco's Modified Eagle Medium (Glutamax) supplemented with 10% fetal bovine serum and 50 μg/mL penicillin/streptomycin at 37°C in a humidified atmosphere of 5% CO_2.

2.2.1 Alamar blue viability assay

HeLa cells were seeded at a density of 5×10^3 cells/well in 96-well plates and treated with the indicated compounds for 24 h. Alamar blue (20 μL) was then added to each well and incubated at 37°C in the dark for 4 h. Plates were then read on a fluorescence plate reader (SpectraMax Gemini, Molecular Devices) with excitement and emission wavelengths of 544 and 590 nm respectively. Experiments were performed in triplicate on three independent days with activity expressed as percentage cell viability compared to vehicle treated controls. All data points (expressed as means±S.E.M.) were analysed using GRAPHPAD Prism (Graphpad software Inc., San Diego, CA).

2.2.2 Confocal microscopy

HeLa cells were seeded at a density of 1×10^5 cells/well in glass bottom wells and treated with the indicated compounds for 24 h. Cells were either imaged straightaway for live imaging or alternatively cells were fixed in 3% paraformaldehyde for 3 min. Samples were then rinsed with PBS and stained with DRAQ5 (red nuclear stain). Samples were then rinsed with a buffer at the indicated pH followed by addition of 0.5 mL of the same pH buffer and imaged by confocal microscopy (Olympus FV1000, 60X oil immersion lens). Samples were then repeatedly rinsed and imaged in subsequent pH buffers, all imaging settings were kept the same throughout the experiment. Image analysis was performed using FluoView Version 7.1 Software. Compounds were excited by a 405 nm argon laser, emission 500–550 nm, DRAQ5 was excited by a 633 nm red helium-neon laser, emission > 650 nm.

2.2.3 Co-localisation studies

Cells were either transfected with a DsRed mitochondrial plasmid for 4 h or a CellLight lysosome-red fluorescent protein (RFP) tag (molecular probes) for 16 h. Cells were then treated for 24 h with 1 μmol·L^{-1} of the indicated compounds, washed twice with fresh media, stained with the nuclear dye DAPI and analysed by live confocal microscopy. DAPI (4′,6-diamidino-2-phenylindole) and the compounds were excited by a 405 nm argon laser, with emission 410–450 nm (DAPI) and 500–550 nm (compounds), DsRed and RFP tags were excited by a 633 nm red helium-neon laser, emission > 650 nm. For emission spectra, samples were activated by a 405 nm laser and any emission from 420 to 685 nm was recorded using a Leica SP8 confocal microscope. Fluorescent intensity for regions of interest (extracellular (background), organelle and compound localisation) were analysed and graphed.

2.3 General procedure

4-Bromo-1,8-naphthalic anhydride (0.200 g, 0.722 mmol) was dissolved in ethanol (5 mL). The correspondent amine (benzylamine/4-aminobenzylamine) was added (0.722 mmol) to the previous solution. This mixture was irradiated in the microwave during one hour, giving rise to a pale yellow solid.

2-Benzyl-6-bromo-1H-benzo[de]isoquinoline-1,3(2H)-dione (**5**) (0.230 g, 97%): m.p. 173°C; ^{1}H-NMR (400 MHz, $(CD_3)_2SO$, δ ppm): 8.58 (d, 1H, CH, J = 8.3 Hz) 8.55 (d, 1H, CH, J = 8.3 Hz), 8.33 (d, 1H, CH, J = 7.9 Hz), 8.20 (d, 1H, CH, J = 7.9 Hz), 8.00–7.95 (m, 1H, CH), 7.32 (d, 2H, CH, J = 7.4 Hz), 7.26 (t, 2H, CH, J = 7.4 Hz), 7.19 (t, J = 7.2 Hz, 1H), 5.22 (s, 2H); ^{13}C-NMR (101 MHz, $(CD_3)_2SO$, δ ppm): 163.06, 137.14, 132.92, 131.92, 131.50, 131.31, 129.42, 128.95, 128.39, 127.54, 127.11, 121.97, 43.05; IR(neat): 1675, 1653, 1588, 1571, 1436, 1369, 1332, 1294, 1231, 1160, 1127, 1069, 951, 816, 774, 746, 694; HR-ESI-MS: Calcd. for $C_{19}H_{12}BrNO_2$ $[M+H]^+$ 366.0051, found 366.0083; Analysis calcd. for $C_{19}H_{12}BrNO_2$: C 61.3, H 3.4, N 3.8; found: C 60.8, H 3.5, N 3.8.

2-(4-Aminobenzyl)-6-bromo-1H-benzo[de]isoquinoline-1,3(2H)-dione **(6)** (0.225 g, 82%): m.p. 224°C; ^{1}H-NMR (400 MHz, $(CD_3)_2SO$, δ ppm): 8.59 (dd, CH, 2H, J = 12.3, 7.9 Hz), 8.37 (d, CH, 1H, J = 7.9 Hz), 8.24 (d, CH, 1H, J = 7.9 Hz), 8.06–7.97 (m, CH, 1H), 7.09 (d, CH, 2H, J = 8.4 Hz), 6.48 (d, CH, 2H, J = 8.4 Hz), 5.07 (s, CH_2, 2H), 5.01 (s, 2H); ^{13}C-NMR (101 MHz, $(CD_3)_2SO$, δ ppm): 163.44, 148.38, 133.29, 132.32, 131.96, 131.72, 130.38, 129.68, 129.63, 129.42, 124.60, 123.27, 114.05, 43.13; IR

(neat): 3476, 3372, 1690, 1651, 1618, 1585, 1515, 1439, 1373, 1335, 1285, 1233, 1181, 951, 851, 781, 748, 715; HR-ESI-MS: Calcd. for $C_{19}H_{14}N_2O_2Br$ $[M+H]^+$ 381.0239, found 381.0243; Analysis calcd. for $C_{19}H_{13}BrN_2O_2$: C 59.9, H 3.4, N 7.3; found: C 59.7, H 3.3, N 7.2.

2.3.1 Synthesis of naphthalimide sensors 2-benzyl-1H-benzo[de]isoquinoline-1,3(2H)-dione (**1**) and 2-(4-aminobenzyl)-1H-benzo[de]isoquinoline-1,3(2H)-dione (**2**)

General procedure. The precursor (**5**)/(**6**) (0.270 mmol) was added to 3 mL (12.09 mmol) of neat triethylenetetramine. The mixture was irradiated in the microwave for 1 h at 120°C giving rise to an orange solution that has been poured over ice. The formation of a gelatinous orange suspension was observed after 12 h. For a good separation centrifugation of the suspension was carried out yielding an orange solid that was extracted to DCM followed by $NaHCO_3$ and brine washes. The organic phase was dried with dried $MgSO_4$ and the volume was reduced under reduced pressure being possible to isolate a pale orange solid.

2-Benzyl-1H-benzo[de]isoquinoline-1,3(2H)-dione (**1**) (0.059 g, 50%): m.p. 192°C; ^{1}H-NMR (400 MHz, $(CD_3)_2SO$, δ ppm): 8.49 (m, 1H, NH) 8.45 (m, 2H, CH), 8.25 (d, 1H, CH, J = 8.6 Hz), 7.87–7.82 (m, 1H, CH) 7.65 (m, 2H, CH), 7.35–7.15 (m, 5H), 5.15 (s, 2H, CH_2), 4.10 (m, 1H, NH_2), 3.43 (bs, 4H, CH_2), 2.84 (t, 2H, NH_2), 2.75 (t, 2H, CH_2), 2.65–2.50 (m, 3H, CH_2), 2.30 (m, 1H, NH); ^{13}C-NMR (101 MHz, $(CD_3)_2SO$, δ ppm): 163.32, 138.35, 134.98, 131.43, 131.33, 128.70, 127.91, 127.71, 127.47, 127.29, 120.55, 107.85, 70.22, 53.27, 44.19, 43.33, 42.89, 17.68; IR(neat): 3347, 3233, 1697, 1656, 1593, 1437, 1380, 1337, 1236, 1078, 950, 825, 780, 763, 706; HR-ESI-MS: Calcd. for $C_{25}H_{29}N_5O_2Na$ $[M+Na]^+$ 454.2213, found 454.2229; Analysis calcd. for $C_{25}H_{29}N_5O_2$: C 69.6, H 6.8, N 16.2; found: C 70.6, H 7.0, N 17.4.

2-(4-Aminobenzyl)-1H-benzo[de]isoquinoline-1,3(2H)-dione (**2**) (0.053g, 45%): m.p. 205°C; ^{1}H-NMR (400 MHz, $(CD_3)_2SO$, δ ppm): 8.49 (m, 1H, NH) 8.45 (m, 2H, CH), 8.25 (d, 1H, CH, J = 8.6 Hz), 7.87–7.82 (m, 1H, CH) 7.65 (m, 2H, CH), 7.03 (m, 2H, CH), 6.92 (d, 1H, CH, J = 8.4 Hz), 6.79 (d, 1H, CH, J = 8.7 Hz), 6.43 (m, CH, 2H), 5.02 (m, 2H, CH_2), 4.93 (d, 2H, NH_2, J = 13.2 Hz), 3.95 (d, 1H, NH, J = 5.5 Hz), 3.43 (bs, 4H, CH_2), 2.83 (t, 2H, NH_2), 2.75–2.50 (m, 8H, CH_2), 2.29 (m, 1H, NH); ^{13}C-NMR (101 MHz, $(CD_3)_2SO$, δ ppm): 164.13, 163.32, 148.09, 134.83, 131.30, 131.19, 129.80, 129.55, 128.46, 127.67, 125.43, 124.79, 124.68, 122.41, 122.27, 114.18, 113.97, 113.92, 112.28, 104.31, 65.33, 53.32, 49.18, 47.67, 43.46, 42.93, 42.46, 15.59; IR(neat): 3443, 3352, 3222, 2922, 1690, 1654, 1584, 1514, 1428, 1380, 1335, 1296, 1238, 1176, 945, 842, 772; HR-ESI-MS: Calcd. for $C_{25}H_{30}N_6O_2Na$ $[M+Na]^+$ 469.2322, found 469.2338; Analysis calcd. for $C_{25}H_{29}N_5O_2$: C 67.2, H 6.8, N 18.8; found: C 66.5, H 7.3, N 17.6.

2.3.2 Synthesis of naphthalimide sensors: 2-benzyl-1H-benzo[de]isoquinoline-1,3(2H)-dione (**3**) and 2-(4-aminobenzyl)-1H-benzo[de]isoquinoline-1,3(2H)-dione (**4**)

General procedure. The precursor (**5**)/(**6**) (0.270 mmol) was added to 3 mL (29.60 mmol) of neat *N*,*N*-Dimethylethylenediamine. The mixture was irradiated in the microwave for 1 h at 120°C giving rise to an orange solution that has been poured over ice. The formation of a gelatinous orange suspension was observed after 12 h. For a good separation centrifugation of the suspension was carried out yielding an orange solid that was extracted to DCM followed by $NaHCO_3$ and brine washes. The organic phase was dried with dried $MgSO_4$ and the volume was reduced under reduced pressure being possible to isolate a pale orange solid.

2-Benzyl-1H-benzo[de]isoquinoline-1,3(2H)-dione (**3**) (0.069 g, 78%): m.p. 177°C; ^{1}H-NMR (400 MHz, $(CD_3)_2SO$, δ ppm): 8.63 (d, J = 8.4 Hz, 1H), 8.41 (d, J = 7.2 Hz, 1H), 8.25 (d, J = 8.5 Hz, 1H), 7.65 (t, J = 7.7 Hz, 2H), 7.26 (m, 4H), 7.18 (d, J = 6.8 Hz, 1H), 6.77 (d, J = 8.6 Hz, 1H), 5.18 (s, 2H), 2.55 (t, J = 6.6 Hz, 2H), 2.19 (s, 6H), 2.11 (s, 2H); ^{13}C-NMR (100 MHz, $(CD_3)_2SO$, δ ppm): 164.23, 163.33, 151.15, 138.36, 134.96, 131.37, 129.94, 129.14, 128.70, 127.89, 127.29, 124.81, 122.16, 120.54, 107.83, 104.38, 57.32, 45.73, 45.45, 42.88, 41.37, 40.55, 40.34, 40.13, 39.93, 39.72, 39.51, 39.30, 31.11; IR(neat): 3336, 3225, 1699, 1652, 1584, 1435, 1384, 1336, 1231, 1088, 953, 835, 782, 762; HR-ESI-MS: Calcd. for $C_{23}H_{24}N_3O_2$ $[M+H]^+$ 374.1790, found 374.1621; Analysis calcd. for $C_{23}H_{23}N_3O_2$: C 74.0, H 6.2, N 11.3; found: C 73.2, H 6.5, N 12.0.

2-(4-Aminobenzyl)-1H-benzo[de]isoquinoline-1,3(2H)-dione (**4**) (0.064 g, 63%): m.p. 197°C; ^{1}H-NMR (400 MHz, $(CD_3)_2SO$, δ ppm): 8.63 (d, J = 8.4 Hz, 1H), 8.43 (d, J = 7.2 Hz, 1H), 8.27 (d, J = 8.5 Hz, 1H), 7.64 (at, J = 8.5, 7.2 Hz, 1H), 7.61 (bs, 1H, CH), 7.06 (d, J = 8.3 Hz, 2H), 6.78 (s, 1H), 6.46 (d, 2H, CH, J = 8.2 Hz), 5.02 (s, 2H, CH_2), 4.94 (m, 2H, NH_2), 3.46 (d, CH_2, 2H, J = 5.9 Hz), 2.58 (t, CH_2, 2H, CH_2, J = 6.7 Hz), 2.23 (s, 6H, CH_3); ^{13}C-NMR (100 MHz, $(CD_3)_2SO$, δ ppm): 164.13, 163.32, 150.96, 148.08, 134.78, 131.20, 129.79, 129.53, 128.92, 128.46, 125.43, 124.75, 122.32, 120.48, 114.19, 113.93, 112.28, 108.08, 104.30, 57.34, 45.74, 42.46, 41.37, 31.11; IR(neat): 3423, 3332, 3220, 2924, 1691, 1645, 1584, 1514, 1431, 1374, 1331, 1296, 1235, 1175, 945, 839, 771; HR-ESI-MS: Calcd. for $C_{23}H_{24}N_4O_2Na$ $[M+Na]^+$ 411.1791, found 411.2103; Analysis calcd. for $C_{23}H_{24}N_4O_2$: C 71.1, H 6.2, N 14.4; found: C 72.2, H 6.8, N 14.8.

3 Results and discussion

3.1 Design and synthesis

The four PET naphthalimide based pH probes **1-4** were designed on the PET principle, and the fluorophores-spacer-receptor concept developed by de Silva [34,35], by incorporating an amino alkyl chain (**1** and **2** triethylenetetramine; **3** and **4** *N*,*N*-dimethylethylenediamine) to the 4-position of the **Nap** moiety, and by incorporating a benzyl unit at the imide site. Our objective was that the benzyl unit would potentially function as a PET quencher, or as a means by which further conjugation of the sensor into biomolecules via coupling of the aniline unit. All were synthesized in two steps in moderate to good yields; this involved the initial condensation of the 4-bromo-1,8-naphthalic anhydride with either benzylamine or 4-aminobenzylamine to give **5** and **6** respectively. This was followed by a substitution of the bromine atom at the 4-position of **5** and **6**, with either neat triethylenetetramine or neat *N*,*N*-dimethylethylenediamine, under microwave irradiation for 1 h at 120°C, yielding orange solutions. This was then followed by precipitation of the desired products upon pouring these solutions over ice, yielding sensors **1-4** in 45%–70% yields (See full assignment in the Experimental Section). These PET sensors were characterised using conventional methods, including NMR and MS. It was noted that in the case of **1** and **2**, the resolution of the ^{1}H NMR indicated that some aggregation occurred in water at high concentrations, but we have seen such a

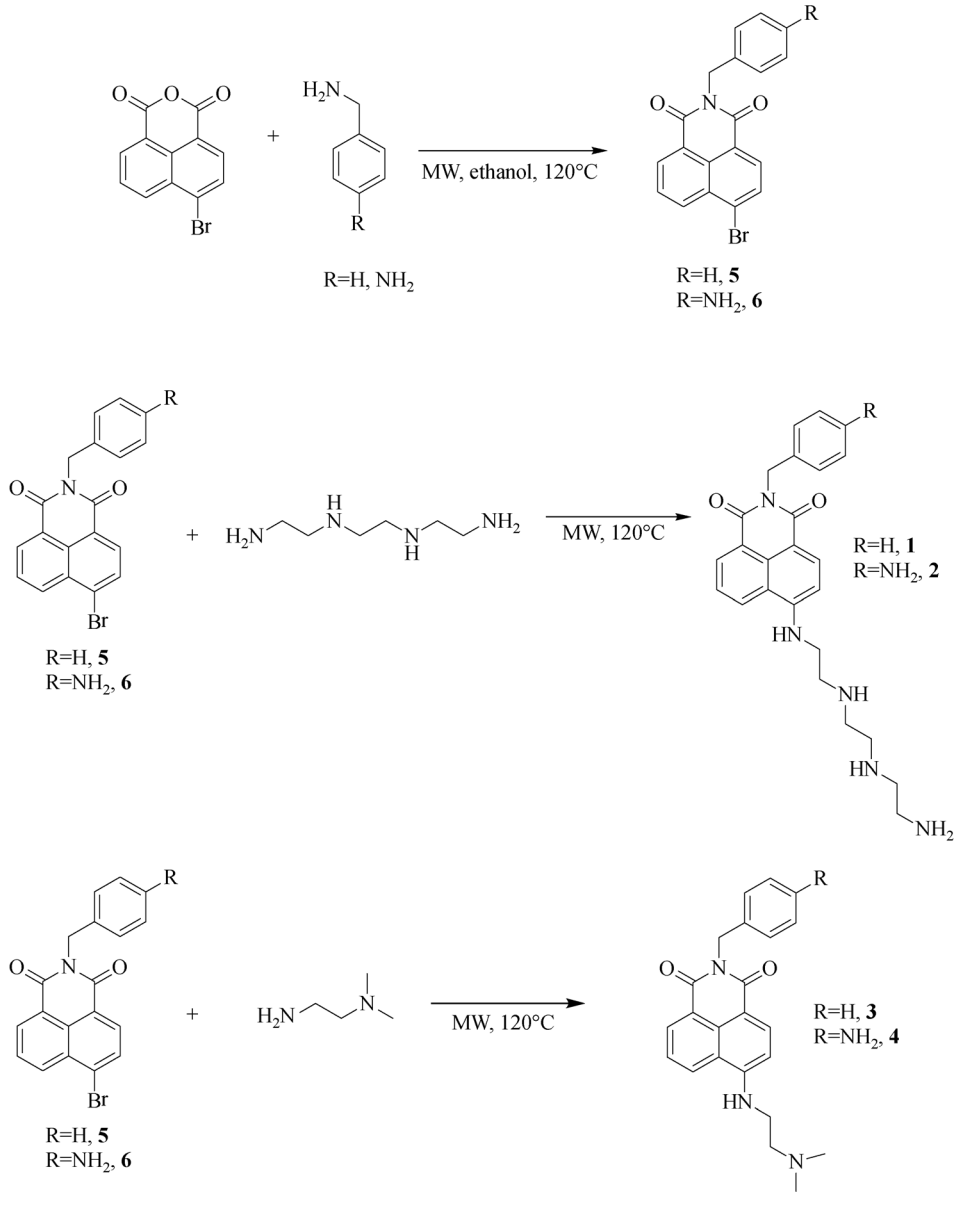

Scheme 1 The synthesis of **NAP** sensors **1-4** developed in this study.

phenomenon recently for other **Nap** based structures, such as those based on glycosylated **Naps** and 1,8-naphthalimide Tröger's bases [36].

3.2 Ground and excited state spectroscopic investigations

Having synthesised **1-4**, their photophysical properties were probed initially in 0.1 $mol \cdot L^{-1}$ NaCl aqueous solutions using 10^{-5} $mol \cdot L^{-1}$ concentrations. In the case of **1** and **2**, the structures gave rise to 'typical' **Nap** based absorptions [37,38]; the UV-Vis absorption spectrum of **1** presents five main bands centred at 230 (ε = 17760 $M^{-1} \cdot cm^{-1}$), 255 (ε = 9680 $M^{-1} \cdot cm^{-1}$), 280 (ε = 9327 $M^{-1} \cdot cm^{-1}$) and the characteristic ICT band of the 4-amino-1,8-naphthalimides at 437 nm (ε = 6680 $M^{-1} \cdot cm^{-1}$). The absorption spectrum of **2** showed the same set of bands at 232 (ε = 20500 $M^{-1} \cdot cm^{-1}$), 255 (ε = 11935 $M^{-1} \cdot cm^{-1}$), 280 (ε = 9420 $M^{-1} \cdot cm^{-1}$) and 437 nm (ε = 7360 $M^{-1} \cdot cm^{-1}$). The same behaviour was observed for sensors **3** and **4** with bands at 255 (ε = 13060 $M^{-1} \cdot cm^{-1}$), 280 (ε = 12480 $M^{-1} \cdot cm^{-1}$), 433 nm (ε = 12300 $M^{-1} \cdot cm^{-1}$), and 253 (ε = 19100 $M^{-1} \cdot cm^{-1}$), 280 (ε = 15300 $M^{-1} \cdot cm^{-1}$), and 433 nm (ε = 13360 $M^{-1} \cdot cm^{-1}$), respectively.

The **Nap** systems are commonly used in biological media due to their rich photophysical properties, which includes long wavelength fluorescent emission. To probe this, compounds **1-4** were excited at their ICT bands (432–437 nm), giving rise in all cases to long wavelength fluorescent emission bands centred at 530 for **1** and 535 nm for **2-4**, typical of such 4-amino-**Nap** structures. The excitation spectra were also recorded for all four structures, all being structurally identical to that seen for these sensors in the absorption spectra. The fluorescence quantum yield (Φ_F) for **1** was determined as 0.67 (in the same media) while for compound **2**, a significantly reduced Φ_F of 0.07 was observed. We attribute these large differences in Φ_F to the different substituents on the aromatic ring attached to the amide group; the amine being more electron rich and possibly more able to participate in PET to the **Nap** fluorophores. This is somewhat unusual as pH PET quenching is normally much weaker form groups located at the imide side as the electron transfer process is hampered by the ICT state [39–41]. Hence, structure **2** could be considered as a $receptor_1$-$spacer_1$-fluorophore-$spacer_2$-$receptor_2$ model, where both receptors can give rise to quenching in the **Nap** centre emission [42]. The fluorescence life-times for sensors **1** and **2** was also measured in same media giving rise to similar values of 5.98±0.02 and 5.32±0.03 ns for **1** and **2**, respectively.

3.3 pH dependent ground and excited state spectroscopic investigations

Having looked at the fundamental photophysical properties of **1-4** we next investigated the changes in the ground and the excited state of these sensors as a function of pH, by carrying out pH titrations from either acidic media to alkaline or alkaline to acidic media. As can be seen from the changes in the absorption spectrum of **1** in Fig. 2(a), significant changes were observed in both the high energy transitions as well in the ICT band from 431 to 448 nm; the absorption being red shifted upon going from acidic to basic media. Similar changes were seen for **2**, Figs. 2(b), c.f. discussion below. In the case of **1**, which has the benzyl unit at the imide side, one would argue that this phenomenon is due to the deprotonation of the secondary amino group at the 'receptor' site attached to 4th position of the **Nap** ring. In its protonated form the ICT is slightly affected due to electrostatic repulsion of the ammonium ion and the 4-amino moiety of the **Nap** ring that has a partial δ^+ due to the 'push-pull' nature of the ICT character [43]. The changes also indicate that some aggregation is being observed and the clear evidence of an isosbestic point is not present. As this sensory system is based on the simpler fluorophore-spacer-receptor model, one would only expect a minor change in the ground state of the

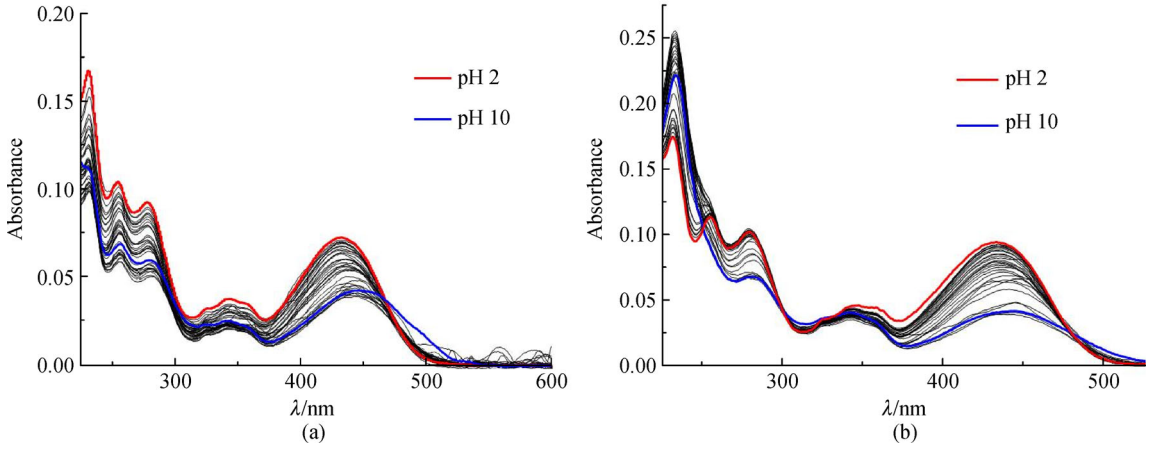

Fig. 2 Absorption spectra of (a) **1** recorded over the titration range from pH 2 to pH 10, demonstrating that a red shift was observed upon moving into alkaline media; (b) The same titration for **2** commencing in acidic solution and titrating with a base.

fluorophores (as the two are covalently separated by a spacer). However, in the case of **1**, these changes are clearly more pronounced than normally seen for simple pH PET sensors. Similar effects, (and even slightly stronger changes) were also seen for **2**, Fig. 2(b), where the same bathochromic shift was observed; in this case being even more pronounced. For both systems, pH titrations from alkaline to acidic media were also undertaken. On both occasions, hyperchromicity was observed, but interestingly enough (without using significant equilibrium times between additions) a somewhat smaller effect was observed. Again, this could be due to some aggregation or slight dilution effects.

To investigate the bathochromic shift seen in alkaline media further, we also carried out pH titrations of **3** and **4**, commencing in acid solution and adding base. Once again, similar changes to that observed for **1** and **2** were seen here, with the absorption being shifted towards the red in alkaline media. This would indicate that the benzyl amine at the imide site has a significant role to play, and hence it is possible that these long wavelength shifts observed, and significant changes in the absorbance, are mainly due to electrostatic interactions between the protonated aniline and the ICT state of the **Nap** moiety, which are more than normally seen for **Nap** systems which have aliphatic units only at the imide site. It has to be also noted that similar effects could has been observed in other naphthalimide derived systems with extended aromatic units at the imide side [44,45]. With this in mind, we next investigated the effect of pH on the fluorescence emission spectra of the compounds **1**-**4** in the same NaCl ionic strength.

For all the sensors, large changes were observed in the fluorescence emission spectra as a function of pH, the emission being 'switched on' in acidic media, due to protonation of any amino moieties that can partake in PET quenching to the **Nap** excited sates due to increased oxidation potential upon protonation of these amines. Upon titration with a base, the emission remained but was slightly affected until pH 3, after which a significant change was observed until pH 8, where the emission was quenched by 75%. These changes were found to be reversible; however, the emission was found to be somewhat reduced in intensity upon carrying out the back titrations, particularly for **1** and **2**. Analysis of these changes at λ_{max} of the ICT transition vs. pH (the profile being shown as inset in Fig. 3(a) for **1**) demonstrated that there is potentially more than just one simple 'sigmoidal step' associated with these pH dependent changes; normally these would take place over 2 pH units, while in the case of **1**, the emission is close to being linearly affected, showing pH dependent luminescence which spans ca. 7 pH units from pH 2 to 9. Taking into account that normally such PET sensors operate by a simple equilibrium and mass-actions, it is clear from the profile that several protonation (or in this case de-protonation) steps are happening.

As the PET quenching can only operate here from the aliphatic amines at the 4-postion of the **Nap** fluorophores, this has to be due to stepwise deprotonation events at this site, which can be affected by conformational changes in the triethylenetetramine unit. While we were unable to determine the pKa values accurately from these changes, it is possible to estimate two pKa values of 4.19 and 6.25 by fitting these changes. We believe that the major changes are due to the presence of the two secondary amines in the triethylenetetramine 'receptor' while the pH changes at the more alkaline pH are possibly due to the distal triethylenetetramine, and as was eluded to above, it is possible that this quenching is due to some degree of folding. Such an effect has been previously described by de Silva and co-workers as being due to a 'steppingstone' pH quenching mechanism [46].

In a similar manner we also carried out pH titrations with sensor **2,** which has an aniline unit at the imide site, which is also pH 'active', and hence, can be considered as a receptor$_1$-spacer$_1$-fluorophore-spacer$_2$-receptor$_2$ model. As

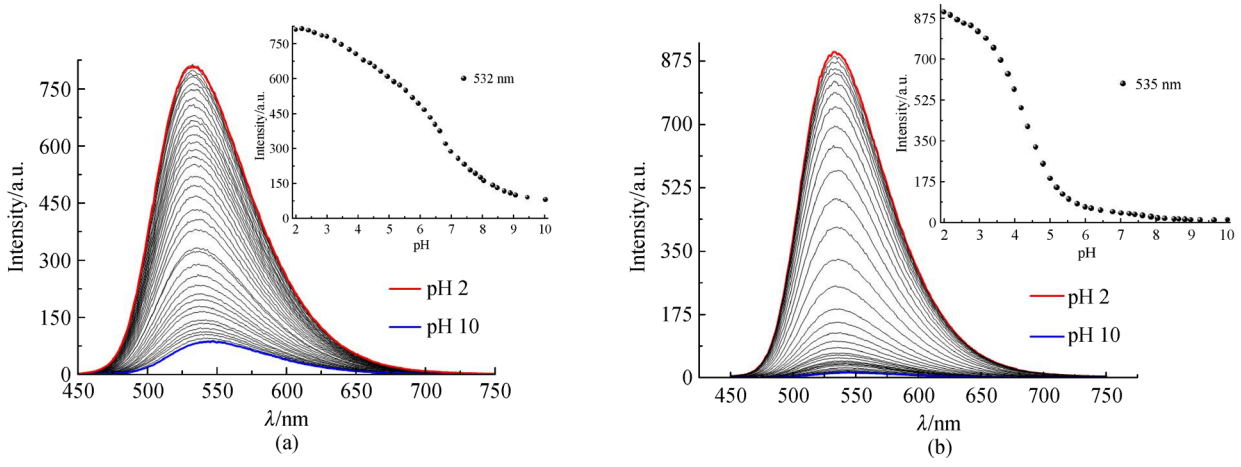

Fig. 3 (a) The overall changes in the fluorescence emission spectra of sensor **1** from pH 2 to 10. Inset: The changes occurring at 535 nm between pH 2 and pH 10; (b) The same changes observed for sensor **2**.

can be seen in Fig. 3(b), the pH titration carried out with the sensor **2** showed more intense changes in the emission spectra recorded giving rise to an almost complete quenching at pH 10 (Fig. 3(b)). It could be observed that as before, the maximum of the emission was again achieved at pH 2. However, the intensity of the emission decreased in a more pronounced manner than **1** in such a way that at pH 5 the emission of **2** has been already quenched by ca. 90% whereas in the case of **1** at the same pH it had been quenched by ca. 20%. Here, clearly the emission quenching was more in line with that observed for systems where a single quenching pathway (which operates over 2 log units) was operating (c.f. the inset in Fig. 3(b)). The profile also demonstrates that the quenching of **2** continued upon further addition of a base giving rise to an almost complete quenching of the emission above pH 8. The predominant sigmoidal step we associated with the protonation of the NH groups at the 4-position of the naphthalene ring corresponding to a pKa of 4.40, in conjunction with that occurring at the receptor$_2$ site. This is somewhat unusual, as normally, the PET transfer is directional [39,43], with the PET being more effective from amines positioned at the 4-amino moiety of the **Nap**, and in line with the push-pull character of the ICT system, rather than from the imide side where the PET is opposed to the push-pull nature of the ICT state. The theoretical examination for this directionality was originally investigated by Gao and Marcus [47] who concluded that this directionality was "due to the difference in the electronic coupling matrix elements (jVj) for the two reactions", and consequently, the electron transfer from the 4-amino side was ~10000 times faster than from the imide side. However, as we observed above, the Φ_F was almost 10 times higher for **1** than **2**, which would indicate that this PET pathway is activated. Nevertheless, we were able to estimate other minor sigmoidal steps in the titration of **2**, which can be assigned to PET processes from the triethylenetetramine receptor. So, while the overall quenching of **1** and **2** is similar, the emission is clearly more stepwise for **1** than **2** which can only be due to the nature of the benzyl groups at the imide sites.

With the view of investigating this further, the pH dependent emission of **3** and **4** was also studied; the difference being that these only have a single protonation site at the 4-amino moiety, the overall titrations and the changes in the λ_{max} of the ICT band as a function of pH being shown in Fig. 4. In the titration carried out with **3**, the same kind of pH dependence as for **1** and **2** was observed; the emission was switched on in acidic media around pH of 3, and ca. 90% 'switched off' in alkaline media. A significant difference was found however, on examining the isotherm plot for the changes at 535 nm, as here, a big sigmoidal step was observed centred at pH 8.1, in contrast with the two sigmoidal steps observed at lower pH values for **1**. Hence, sensor **3** behaves as would be seen in 'traditional' **Nap** based pH sensors, and the back titration (from base to acid media) was found to be, to a greater extent, fully reversible within the timeframe of the titration. This would thus point to a higher acidity of the group involved in the acid/base equilibrium in sensor **1**, caused by (i) the presence of the triethylenetetramine chain in the molecule (each protonation event being more difficult to achieve due to the stepwise protonation of the triethylenetetramine moieties), and (ii) that the ICT character of the **Nap** fluorophores in **1**, which induces significant repulsion, is more strongly felt because of it in **1** vs. **3**. When the titration was performed using **4**, the same behaviour was observed (Fig. 4(b)). However, the most significant difference in the emission of **4**, vs. **3**, and that seen for **2**, was the formation of a unique sigmoidal step in the isothermal plot at 535 nm (inset in Fig. 4(b)) that occurred within acidic pH, being centred at pH 4.3. This would indicate that the 4-amino-aniline moiety is the most likely source of the PET quenching in **4** and subsequently

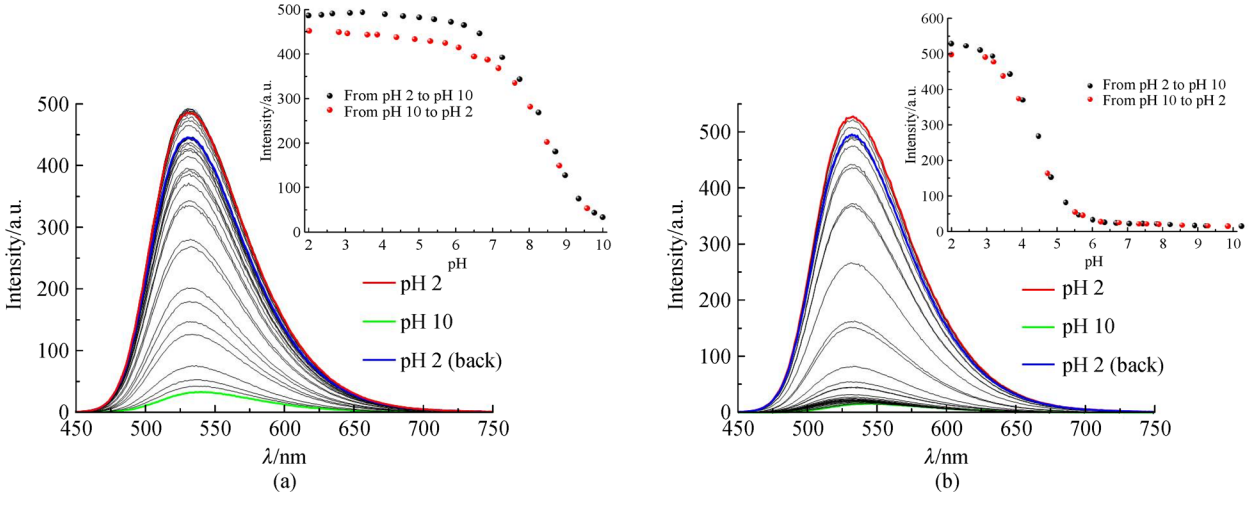

Fig. 4 (a) The overall changes in the emission spectra of sensor **3** from pH 2 to 10 (Inset: The changes occurring at 535 nm between pH 2 and pH 10); (b) The same changes observed for sensor **4**.

in the triethylenetetramine based sensor **2**, and that while **1** and **3** can be described as fluorophore-spacer-receptor systems, **2** and **4** are better described by the receptor$_1$-spacer$_1$-fluorophore-spacer$_2$-receptor$_2$ model; the PET process in **4** being dominated by the benzyl moiety. In summary, the above investigation demonstrates that a minor functionalization of the sensor structure can have significant effects on the photophysical properties of the resulting molecules. Having established that both **1** and **2** gave rise to significant changes in their pH dependent emission, which occurred within acidic media, we next set out to investigate if these structures could be employed as imaging agents within cells for changes in acidic organelles such as lysosomes.

3.4 Cellular imaging studies of **1-4**

The high Φ_F, photostability and pH tuneable nature of the four PET sensors developed herein and, particularly, the significant changes in their pH dependent fluorescent emission within acidic media, of **1** and **2**, makes them potential candidates as targeting imaging agents for pH changes within cancer cells. As a result, the PET naphthalimide based pH probes **1-4** were tested against a common cancer cell line, HeLa cells, for cytotoxic and imaging potential. All the compounds were shown to effect reduced cellular viability of HeLa cells after a 24 h treatment with a range of concentrations of the indicated compounds in a 96-well plate. After the required incubation period, Alamar blue dye (20 μL) was added to each well and samples were incubated for 4 h. Cells were subsequently analysed for cell viability with IC_{50} values ranging from 7.4 μmol·L^{-1}, for compound **4** to 30 μmol·L^{-1}, for compound **2** (Table 1).

Table 1 Cellular viability studies for compounds **1-4** in HeLa cells. A. HeLa cells B. and IC_{50} values for each compound (Values represent the mean of three independent experiments performed in triplicate)

Compound	IC_{50} values /(μmol·L^{-1})
1	16.0
2	30.0
3	13.1
4	7.41

Having established that using low concentrations of these agents would potentially facilitate their pH imaging application, we next employed them in confocal microscopy experiments using living cancer cells, which were treated with 25 μmol·L^{-1} of these compounds. The results for **1** and **2** in cervical cancer (HeLa) cells that were treated for 24 h before imaging are shown in Fig. 5, under physiological pH conditions using the nuclear stain DRAQ5, but the absorption and the emission spectra of this stain did not overlap with the long **Nap** wavelength in

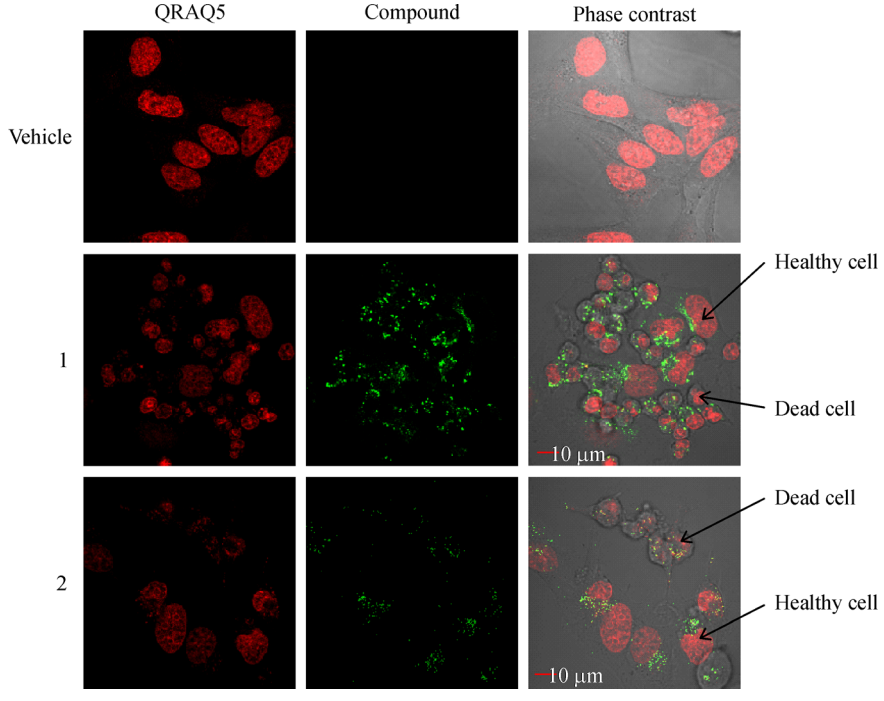

Fig. 5 Confocal fluorescence imaging for the pH PET sensors **1** and **2** within HeLa cells that were treated for 24 h with the indicated compounds, upon excitation by a 405 nm argon laser, collecting the emission between 500−550 nm; Nap emission being observed as green fluorescence emission. After the required incubation period, cells were also stained with the nuclear stain DRAQ5, which was subsequently excited by a 633 nm red helium-neon laser, emission > 650 nm using live confocal microscopy, and shown as red emission. Images are representative of three independent experiments.

this media. The results demonstrate that the compound fluorescence appeared localised to the cytoplasm and this is consistent with other **Nap** based structures developed by our group. Images for living cells treated with **1** and **2** (25 μmol·L^{-1}) showed that some cells undergo apoptosis as indicated by cellular shrinkage, condensed chromatin and the formation of apoptotic bodies, all characteristic features of apoptosis. However, **1** did display a higher level of toxicity than **2** that agrees with the cellular toxicity results showing sensor **1** to be more potent in Fig. 5. Hence, with the view of employing these **Nap** sensors as fluorescent imaging agents, the concentration would have to be lower. With this in mind, and with a view to investigating if **1** and **2** could be employed to image pH changes within cervical cancer cells, we also imaged fixed HeLa cells that were treated at a lower concentration of **1** and **2** of 1 μmol·L^{-1} in different pH buffers. These experiments were carried out using the nuclear stain DRAQ5, which did not show changes in the absorption and the emission spectra in acidic or at neutral pH, though at more alkaline pH, the DRAQ5 observed a slight red shift in the absorption and emission, however, these were not accompanied by enhancement in the emission intensity. The results are shown in Figs. 6(a) and 6(b) for **1** and **2**, respectively, and clearly demonstrate that no toxicity is observed when the cells were treated at this lower concentration, and that the fluorescence is highly pH sensitive within the cellular media. Comparing **1** and **2** at different pHs, it is clear that while both systems can report changes in the intracellular pH, sensor **1** is more emissive at elevated pH values (such as between pH 6–8) than **2**, which is significantly more emissive at lower pH values (between pH 2–4). This agrees with the pH dependent fluorescence and the pH profiles observed above and shown in Fig. 3. It is also worth pointing out that even though both sensors are somewhat emissive at medium to alkaline pH 8–10, the fluorescence

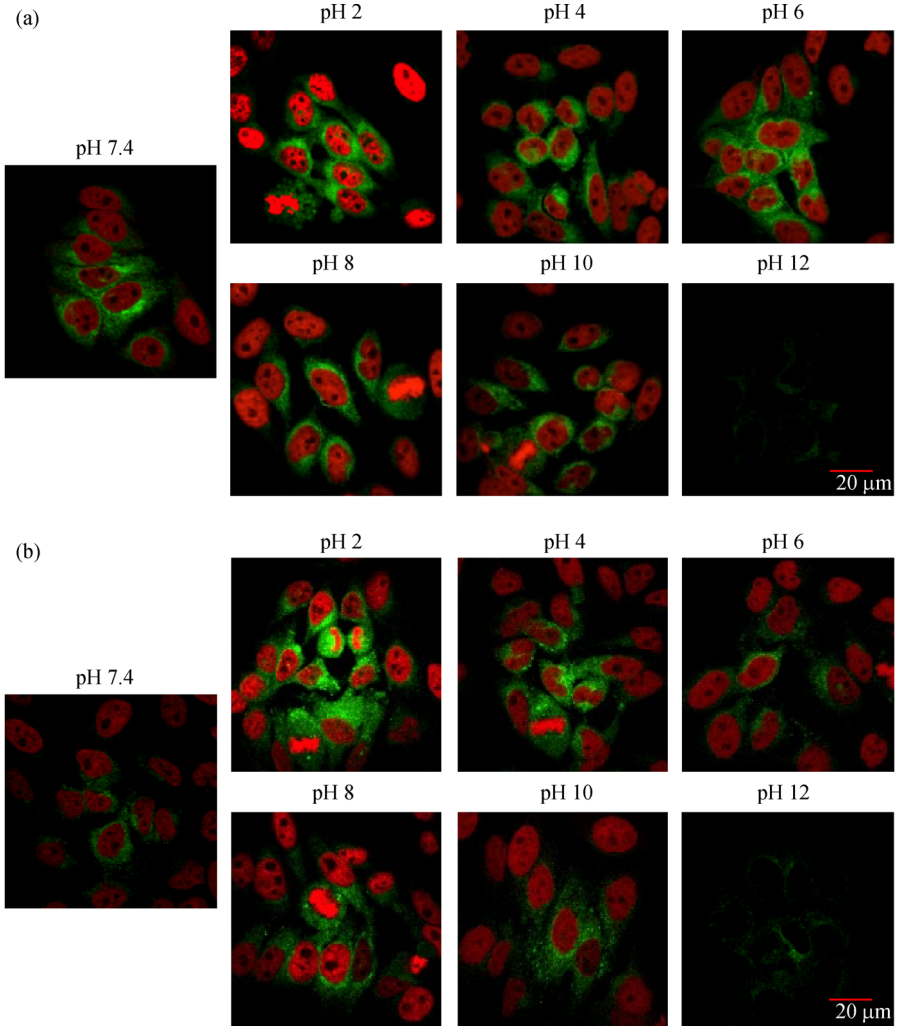

Fig. 6 Confocal fluorescence imaging for the pH PET sensors (a) **1** and (b) **2** at 1 μmol·L^{-1}, within fixed HeLa cells, which were treated for 24 h with the indicated compounds. After the required incubation period, cells were fixed in 3% paraformaldehyde and stained with the nuclear stain DRAQ5. Samples were rinsed and imaged with buffers at the indicated pH. **1** and **2** were excited by a 405 nm argon laser, emission 500−550 nm, while DRAQ5, was excited by a 633 nm red helium-neon laser, emission > 650 nm.

emission is in comparison 'switched off' at pH 12 as the PET process is most active within that media.

In a similar manner the PET sensors **3** and **4** were also imaged under identical conditions to that above, and as shown in Figs. 7(a) and 7(b), respectively, both sensors gave rise to some degree of pH dependent emission. The luminescence arising from compound **3** was found to be significantly less than that seen for **4** in acidic media, and fully quenched at above pH 8. The results demonstrate that both sets of sensors are clearly able to report on the differences in pH within the cell, the most significant changes being observed for **1** and **2**.

In order to further investigate the nature of this pH dependence, intracellular localisation studies were next undertaken within HeLa cells using both **1** and **2**, using DsRed mitochondrial plasmid and a CellLight lysosome-(RFP) tags. Live cell imaging with fluorescently labelled mitochondria and lysosome stains was undertaken, where such cells were treated with sub-toxic concentrations of either **1** or **2** and imaged. The results are shown in Fig. 8 for both compounds (Figs. 8(a) and 8(b), respectively), demonstrating that **1** and **2** appeared to localise with lysosomes, using DAPI as a nuclear stain. The emission spectra of each compound were also recorded in the area of the cell where lysosomes were associated and results displayed fluorescence maxima at 518 and 546 nm for compound **1** and 504 and 546 nm for compound **2** (Fig. 8 (c)). Interestingly, at 530/535 nm, the maxima of the compounds in solution, there was a reduction in the fluorescent intensity, highlighting the impact that the microenvironments of cells have on the photophysical properties of the compounds. In contrast to lysosomal co-

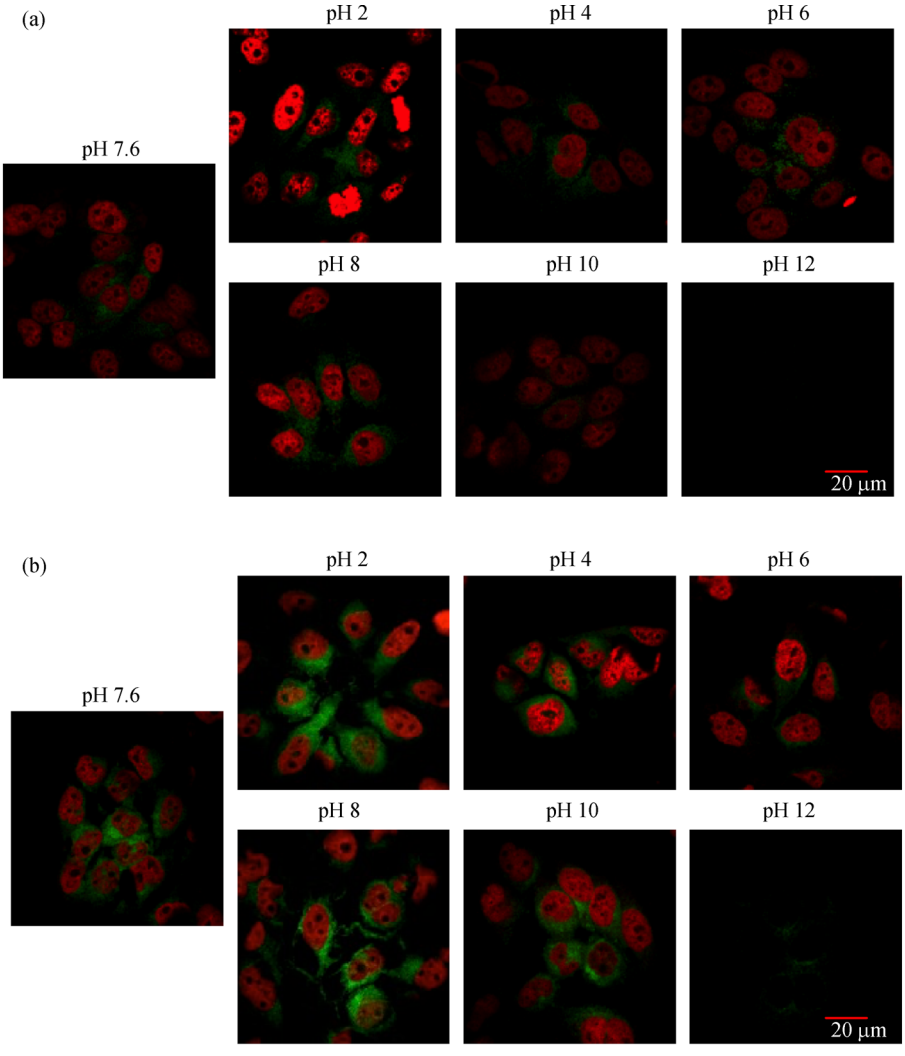

Fig. 7 Confocal fluorescence imaging for the pH PET sensors (a) **3** and (b) **4** at 1 μmol·L^{-1}, within fixed HeLa cells, which were treated for 24 h with the indicated compounds. After the required incubation period, cells were fixed in 3% paraformaldehyde and stained with the nuclear stain DRAQ5. Samples were rinsed and imaged with buffers at the indicated pH. **4** and **5** were excited by a 405 nm argon laser, emission 500−550 nm, while DRAQ5, was excited by a 633 nm red helium-neon laser, emission > 650 nm.

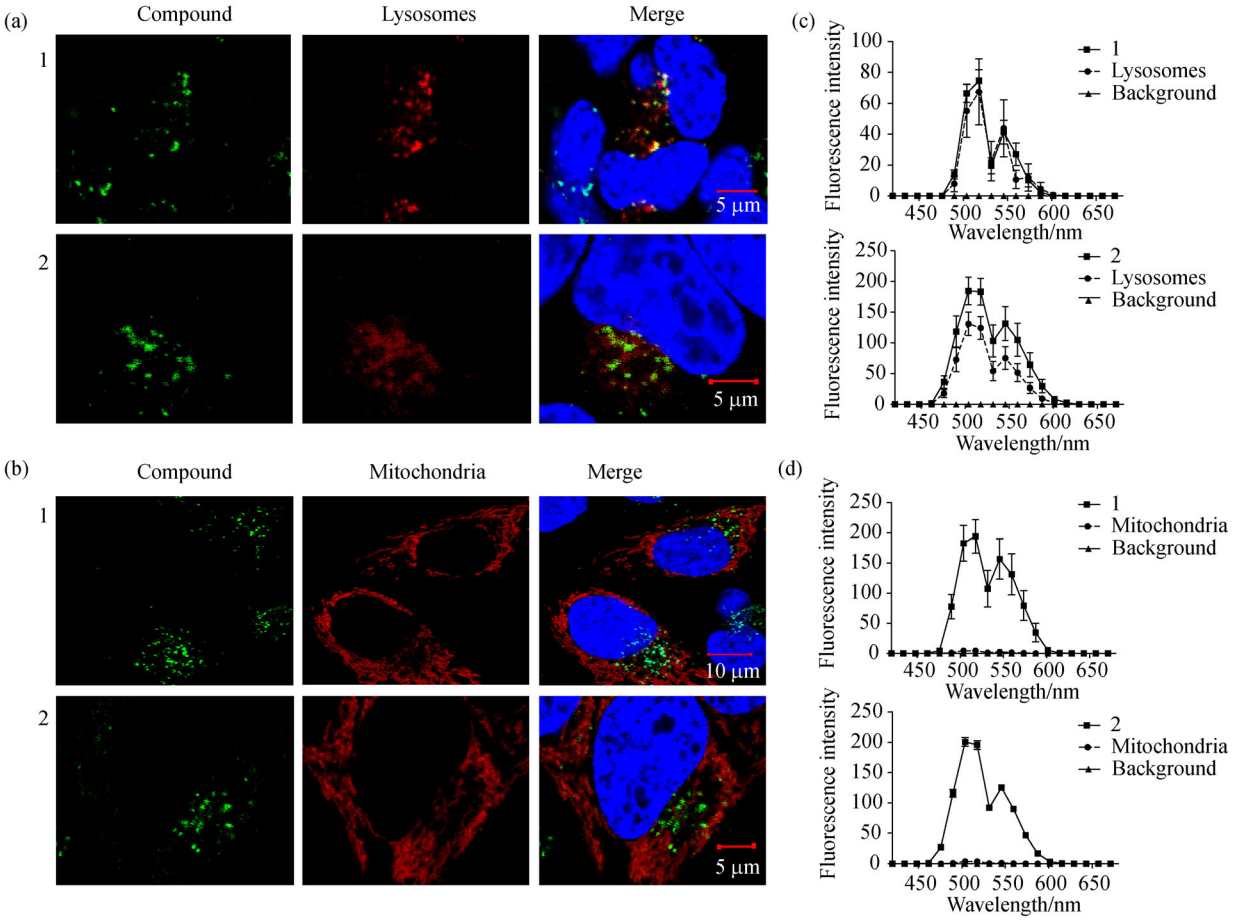

Fig. 8 Confocal fluorescence imaging of (a) **1** and (b) **2** at 1 μmol·L^{-1} in HeLa cells with fluorescently labelled lysosomes and mitochondria stains. These were treated for 24 h with the indicated compounds, washed twice with fresh media and analysed by live confocal microscopy. For images (a), (b) cells were counterstained with DAPI. DAPI and the compounds were excited by a 405 nm argon laser, with emission 410−450 nm (DAPI) and 500−550 nm (compounds), DsRed and RFP tags were excited by a 633 nm red helium-neon laser, emission > 650 nm. For emission spectra, shown in (c) and (d) for **1** and **2** in the two media, were activated by a 405 nm laser and any emission from 420 to 685 nm was recorded using a Leica SP8 confocal microscope.

localisation, and as can be seen in Fig. 8(b), no emission was observed in the area of the cell where mitochondria were associated (Figs. 8(b,d)). The results demonstrating that both **1** and **2** can be employed as pH sensors within cells and as reporter imaging agents for lysosomal pH.

4 Conclusions

Herein, four fluorescent **Nap** molecules were designed and synthesized as pH sensors and cellular imaging agents. We have studied the pH dependence of **1-4** and demonstrated that the fluorescent emissions of all four are highly pH dependent. The results demonstrated that the presence of the benzyl moiety at the imide site has significant effect on the pH dependent PET quenching; particularly for **2** and **4**. For all the systems the emission was 'switched on' in acidic media. For **1**, the titration from acidic media to alkaline almost displayed what is best described as close to a liner dependence from pH 2 → 8, while for **2** the changes were much sharper, mimicking that normally seen for classical fluorescent pH sensors, where the emission is 'switched' over two pH units within acidic media. In both cases we were able to fit the spectroscopic data to give estimated pKa values, which we employed to understand the nature, or the directionality, of the PET quenching. We concluded from this investigation that the 4-amino moiety of the benzyl group in **2** was strongly involved in PET quenching; the electron rich moiety functioning as a second H^+ receptor, with a pKa around 4.5; while for **2**, the PET could only occur from the triethylenetetramine site. Hence, the design of **1** can be described as a classical fluorophore-spacer-receptor model, where, nonetheless, the benzyl amine has significant effect on the overall PET process and due to electron repulsion. In the case of **2** the design is better described as a receptor$_1$-spacer$_1$-fluorophore-spacer$_2$-receptor$_2$ model, where directional quenching from the aniline moiety initially overwrites the PET

from the triethylenetetramine 'receptors' to a greater extent in acidic media, though at less alkaline pH, the PET is operating from receptor$_2$ site as well. In a similar manner, this was also observed for **3** and **4**, designed on the fluorophore-spacer-receptor model and possessing a *N*,*N*-dimethylethylenediamine unit as the H^+ receptor, as here a clear distinction was seen between the benzyl and the 4-amino-benzyl groups; the emission from **3** being only quenched in alkaline solution while for **4** the emission significantly quenched in acidic media (mimicking that seen for **2**). Hence, here directional PET quenching is clearly operating, the pathways being directed by the nature of the benzyl group.

Having established the pH dependent luminescence of **1-4** we carried out both toxicity studies and localisation studies of these compounds within cervical cancer (HeLa) cells. These HeLa cell assays demonstrated the potential of these compounds as cytotoxic agents, where the compounds were able to induce apoptosis at elevated $\mu mol \cdot L^{-1}$ concentrations. However, at 1 $\mu mol \cdot L^{-1}$ concentrations, no such apoptosis was observed, and all the sensors were clearly present within the cytosol. Using confocal fluorescence microscopy and co-localisation studies we were able to confirm that **1** and **2** (as well as **3** and **4**, data not shown) localised within the lysosomes and that these sensors could in fact be used as fluorescence lysosomal imaging probes where changes in the intracellular pH were clearly communicated through direct changes in the fluorescence intensity of these sensors; the emission being highly pH dependent within acidic to neutral pH (the changes within the cellular media mirroring that seen in solution). This is to the best of our knowledge the first example of the use of **Nap** PET sensors that break the rule of 'directional PET quenching' for cellular imaging. We are currently evaluating and developing this area of research [48,49] further for practical biochemical applications of the probes *in vivo*.

Acknowledgements We thank Science Foundation Ireland (SFI PI Award 13/IA/1865 to TG) and TCD for financial support. We also thank the Ministerio of Economía y Competitividad of Spain and The Irish Research Council (IRC) for the funding of postdoctoral fellowships to MMC and AFH (GOIPD/2018/162), respectively. We thank Dr J. E. O'Brien, M. Reuther and G. Hessman (School of Chemistry, TCD) for assisting with NMR and MS.

References

1. Wu D, Sedgwick A C, Gunnlaugsson T, Akkaya E U, Yoon J, James T D. Fluorescent chemosensors: The past, present and future. Chemical Society Reviews, 2017, 46(23): 7105–7123
2. Chang C J, Gunnlaugsson T, James T D. Sensor targets. Chemical Society Reviews, 2015, 44(13): 4176–4178
3. Casey J R, Grinstein S, Orlowski J. Sensors and regulators of intracellular pH. Nature Reviews. Molecular Cell Biology, 2010, 11 (1): 50–61
4. Clark H A, Hoyer M, Philbert M A, Kopelman R. Optical nanosensors for chemical analysis inside single living cells. 1. Sensors for pH and calcium and the intracellular application of PEBBLE sensors I. Analytical Chemistry, 1999, 71(21): 4831–4836
5. Veale E B, Gunnlaugsson T. Fluorescent sensors for ions based on organic structures. Annual Reports Section "B" (Organic Chemistry), 2010, 106: 376–406
6. Han J, Burgess K. Indicators for intracellular pH. Chemical Reviews, 2010, 110(5): 2709–2728
7. Daly B, Ling J, de Silva A P. Current developments in fluorescent PET (photoinduced electron transfer) sensors and switches. Chemical Society Reviews, 2015, 44(13): 4203–4211
8. Duke R M, Veale E B, Pfeffer F M, Kruger P E, Gunnlaugsson T. Colorimetric and fluorescent anion sensors: An overview of recent developments in the use of 1,8-naphthalimide-based chemosensors. Chemical Society Reviews, 2010, 39(10): 3936–3953
9. Banerjee S, Veale E B, Phelan C M, Murphy S A, Tocci G M, Gillespie L J, Frimannsson D O, Kelly J M, Gunnlaugsson T. Recent advances in the development of 1,8-naphthalimide based DNA targeting binders, anticancer and fluorescent cellular imaging agents. Chemical Society Reviews, 2013, 42(4): 1601–1618
10. Shanmugaraju S, la Cour Poulsen B, Arisa T, Umadevi D, Dalton H L, Hawes C S, Savyasachi A J, Watson G W, Williams D C, Gunnlaugsson T. Synthesis, structural characterisation and anti-proliferative activity of a new fluorescent 4-amino-1,8-naphthalimide Tröger's base-Ru(II)-curcumin organometallic conjugate. Chemical Communications, 2018, 54(33): 4120–4123
11. Shanmugaraju S, Hawes C S, Savyasachi A J, Blasco S, Kitchen J A, Gunnlaugsson T. Supramolecular coordination polymers using a close to 'V-shaped' fluorescent 4-amino-1,8-naphthalimide Tröger's base scaffold. Chemical Communications, 2017, 53(93): 12512–12515
12. Shanmugaraju S, McAdams D, Pancotti F, Hawes C S, Veale E B, Kitchen J A, Gunnlaugsson T. One-pot facile synthesis of 4-amino-1,8-naphthalimide derived Tröger's bases via a nucleophilic displacement approach. Organic & Biomolecular Chemistry, 2017, 15(35): 7321–7329
13. Shanmugaraju S, Dabadie C, Byrne K, Savyasachi A J, Umadevi D, Schmitt W, Kitchen J A, Gunnlaugsson T. A supramolecular Tröger's base derived coordination zinc polymer for fluorescent sensing of phenolic-nitroaromatic explosives in water. Chemical Science (Cambridge), 2017, 8(2): 1535–1546
14. Tian Y, Su F, Weber W, Nandakumar V, Shumway B R, Jin Y, Zhou X, Holl M R, Johnson R H, Meldrum D R. A series of naphthalimide derivatives as intra and extracellular pH sensors. Biomaterials, 2010, 31(29): 7411–7422
15. Ao X, Bright S A, Taylor N C, Elmes R B P. 2-Nitroimidazole based fluorescent probes for nitroreductase; monitoring reductive stress in cellulo. Organic & Biomolecular Chemistry, 2017, 15(29): 6104–6108
16. Jia T, Fu C, Huang C, Yang H, Jia N. Highly sensitive naphthalimide-based fluorescence polarization probe for detecting cancer cells. ACS Applied Materials & Interfaces, 2015, 7(18): 10013–10021
17. Lee M H, Han J H, Kwon P S, Bhuniya S, Kim J Y, Sessler J L, Kang C, Kim J S. Hepatocyte-targeting single galactose-appended

naphthalimide: A tool for intracellular thiol imaging *in vivo*. Journal of the American Chemical Society, 2012, 134(2): 1316–1322

18. Dong L, Zang Y, Zhou D, He X P, Chen G R, James T D, Li J. Glycosylation enhances the aqueous sensitivity and lowers the cytotoxicity of a naphthalimide zinc ion fluorescence probe. Chemical Communications, 2015, 51(59): 11852–11855
19. Li X, Lin Y, Wang Q, Yuan Y, Zhang H, Qian X. The novel anti-tumor agents of 4-triazol-1,8-naphthalimides: Synthesis, cytotoxicity, DNA intercalation and photocleavage. European Journal of Medicinal Chemistry, 2011, 46(4): 1274–1279
20. Zhang L, Lei K, Zhang J, Song W, Zheng Y, Tan S, Gao Y, Xu Y, Liu J, Qian X. One small molecule as a theranostic agent: Naphthalimide dye for subcellular fluorescence localization and photodynamic therapy *in vivo*. MedChemComm, 2016, 7(6): 1171–1175
21. Banerjee S, Kitchen J A, Gunnlaugsson T, Kelly J M. The effect of the 4-amino functionality on the photophysical and DNA binding properties of alkyl-pyridinium derived 1,8-naphthalimides. Organic & Biomolecular Chemistry, 2013, 11(34): 5642–5655
22. Banerjee S, Kitchen J A, Gunnlaugsson T, Kelly J M. Synthesis and photophysical evaluation of a pyridinium 4-amino-1,8-naphthalimide derivative that upon intercalation displays preference for AT-rich double-stranded DNA. Organic & Biomolecular Chemistry, 2012, 10(15): 3033–3043
23. Li M, Guo Z, Zhu W, Marken F, James T D. A redox-activated fluorescence switch based on a ferrocene–fluorophore–boronic ester conjugate. Chemical Communications, 2015, 51(7): 1293–1296
24. Li M, Ge H, Mirabello V, Arrowsmith R L, Kociok-Kohn G, Botchway S W, Zhu W, Pascu S I, James T D. Lysosomal tracking with a cationic naphthalimide using multiphoton fluorescence lifetime imaging microscopy. Chemical Communications, 2017, 53(81): 11161–11164
25. Li M, Ge H, Arrowsmith R L, Mirabello V, Botchway S W, Zhu W, Pascu S I, James T D. Ditopic boronic acid and imine-based naphthalimide fluorescence sensor for copper(II). Chemical Communications, 2014, 50(80): 11806–11809
26. Hearn K N, Nalder T D, Cox R P, Maynard H D, Bell T D M, Pfeffer F M, Ashton T D. Modular synthesis of 4-aminocarbonyl substituted 1,8-naphthalimides and application in single molecule fluorescence detection. Chemical Communications, 2017, 53(91): 12298–12301
27. Fleming C L, Natoli A, Schreuders J, Devlin M, Yoganantharajah P, Gibert Y, Leslie K G, New E J, Ashton T D, Pfeffer F M. Highly fluorescent and HDAC6 selective scriptaid analogues. European Journal of Medicinal Chemistry, 2019, 162: 321–333
28. Spiteri J C, Johnson A D, Denisov S A, Jonusauskas G, McClenaghan N D, Magri D C. A fluorescent AND logic gate based on a ferrocene-naphthalimide-piperazine format responsive to acidity and oxidizability. Dyes and Pigments, 2018, 157: 278–283
29. Spiteri J C, Denisov S A, Jonusauskas G, Klejna S, Szacilowski K, McClenaghan N D, Magri D C. Molecular engineering of logic gate types by module rearrangement in 'Pourbaix sensors': The effect of excited-state electric fields. Organic & Biomolecular Chemistry, 2018, 16(34): 6195–6201
30. Johnson A D, Paterson K A, Spiteri J C, Denisov S A, Jonusauskas G, Tron A, Magri D C. Water-soluble naphthalimide-based "Pourbaix sensors": pH and redox-activated fluorescent AND logic gates based on photoinduced electron transfer. New Journal of Chemistry, 2016, 40(12): 9917–9922
31. Banerjee S, Kitchen J A, Bright S A, O'Brien J E, Williams D C, Kelly J M, Gunnlaugsson T. Synthesis, spectroscopic and biological studies of a fluorescent Pt(II) (terpy) based 1,8-naphthalimide conjugate as a DNA targeting agent. Chemical Communications, 2013, 49(76): 8522–8524
32. Calatrava-Pérez E, Bright S A, Achermann S, Moylan C, Senge M O, Veale E B, Williams D C, Gunnlaugsson T, Scanlan E M. Glycosidase activated release of fluorescent 1,8-naphthalimide probes for tumor cell imaging from glycosylated 'Pro-probes'. Chemical Communications, 2016, 52(89): 13086–13089
33. Elmes R B P, Erby M, Bright S A, Williams D C, Gunnlaugsson T. Photophysical and biological investigation of novel luminescent Ru (II)-polypyridyl-1,8-naphthalimide Tröger's bases as cellular imaging agents. Chemical Communications, 2012, 48(20): 2588–2590
34. Zheng S, Lynch P L M, Rice T E, Moody T S, Gunaratne H Q N, de Silva A P. Structural effects on the pH-dependent fluorescence of naphthalenic derivatives and consequences for sensing/switching. Photochemical & Photobiological Sciences, 2012, 11(11): 1675–1681
35. Daly B, Ling J, de Silva A P. Current developments in fluorescent PET (photoinduced electron transfer) sensors and switches. Chemical Society Reviews, 2015, 44(13): 4203–4211
36. Calatrava-Pérez E, Delente J M, Shanmugaraju S, Hawes C S, Williams C D, Gunnlaugsson T, Scanlan E M. Glycosylated naphthalimides and naphthalimide Tröger's bases as fluorescent aggregation probes for Con A. Organic & Biomolecular Chemistry, 2019, 7(8): 2116–2125
37. Duke R M, Gunnlaugsson T. 3-Urea-1,8-naphthalimides are good chemosensors: A highly selective dual colorimetric and fluorescent ICT based anion sensor for fluoride. Tetrahedron Letters, 2011, 52 (13): 1503–1505
38. Gunnlaugsson T, McCoy C P, Morrow R J, Phelan C, Stomeo F. Towards the development of controllable and reversible 'on-off' luminescence switching in soft-matter: Synthesis and spectroscopic investigation of 1,8-naphthalimide-based PET (photoinduced electron transfer) chemosensors for pH in water-permeable hydrogels. ARKIVOC, 2003, 7: 216–228
39. de Silva A P, Gunaratne H Q N, Habib-Jiwan J L, McCoy C P, Rice T E, Soumillion J P. New fluorescent model compounds for the study of photoinduced electron transfer: The influence of a molecular electric field in the excited state. Angewandte Chemie International Edition in English, 1995, 34(16): 1728–1731
40. Veale E B, Gunnlaugsson T. Bi-directional photoinduced electron transfer (PET) quenching is observed in 4-amino-1,8-naphthalimide based fluorescent anion sensors. Journal of Organic Chemistry, 2008, 73(20): 8073–7076
41. Rice T E, de Silva A P. A small supramolecular system which emulates the unidirectional, path-selective photoinduced electron transfer (PET) of the bacterial photosynthetic reaction centre (PRC). Chemical Communications, 1999: 163–164
42. Magri D C, de Silva A P. From PASS 1 to YES to AND logic: Building parallel processing into molecular logic gates by sequential

addition of receptors. New Journal of Chemistry, 2010, 34(3): 476–481

43. Veale E B, Kitchen J A, Gunnlaugsson T. Fluorescent tren-based 4-amino-1,8-naphthalimide sensor for Cu(II) based on the use of the (fluorophore-spacer-receptor) photoinduced electron transfer (PET) principle. Supramolecular Chemistry, 2013, 25(2): 101–108
44. Qian J, Xu Y, Qian X, Wang J, Zhang S. Effects of anionic surfactant SDS on the photophysical properties of two fluorescent molecular sensors. Journal of Photochemistry and Photobiology A Chemistry, 2008, 200(2-3): 402–409
45. Zhou L, Jin Z, Fan X, Yao Y, Zhaoyang C, Zhang W, Qian J. Synthesis of 1,8-naphthalimide-based fluorescent nano-probes and their application in pH detection. Chinese Chemical Letters, 2018, 29(10): 1500–1502
46. de Silva A P, Gunaratne H Q N, Gunnlaugsson T, Lynch P L M. Molecular photoionic switches with an internal reference channel for fluorescent pH sensing applications. New Journal of Chemistry, 1996, 20(7-8): 871
47. Gao Y Q, Marcus R A. Theoretical investigation of the directional electron transfer in 4-aminonaphthalimide compounds. Journal of Physical Chemistry A, 2002, 106(10): 1956–1960
48. Veale E B, Gunnlaugsson T. Synthesis, photophysical and DNA binding studies of fluorescent Tröger's base derived 4-amino-1,8-naphthalimide supramolecular clefts. Journal of Organic Chemistry, 2010, 75(16): 5513–5525
49. Ryan G J, Poynton F E, Elmes R B P, Erby M, Williams D C, Quinn S J, Gunnlaugsson T. Unexpected DNA binding properties with correlated downstream biological applications in mono vs. bis-1,8-naphthalimide Ru(II)-polypyridyl conjugates. Dalton Transactions (Cambridge, England), 2015, 44(37): 16332–16344